IOP Publishing | Vietnam Academy of Science and Technology Advances in Natural Sciences: Nanoscience and Nanotechnology
Adv. Nat. Sci.: Nanosci. Nanotechnol. 11 (2020) 035009 (8pp) https://doi.org/10.1088/2043-6254/ab9d1d

Effect of hybrid nanofluids on thermal and hydraulic characteristics of hexagon tube

Kadhim Fadhil Nasir, Haider R D Al-Hamadani[1] and Hassan Ali Jurmut

Al-Furat Al-Awsat Technical University, Al-Musaib Technical College, Department of Machines and Equipment Engineering Techniques, Babil, Iraq

E-mail: kad2020@atu.edu.iq, dr.haider.alhamadani@atu.edu.iq and com.hyd1@atu.edu.iq

Received 8 January 2020
Accepted for publication 20 March 2020
Published 2 July 2020

Abstract

The commonly determinations of present study are evaluation numerically the thermal transfer and hydraulic distribution inside the turbulent flow pattern for Al_2O_3-water nanofluids and hybrids fluid of (Al_2O_3 and CuO) dispersed in pure water concluded a straight hexagon pipe with constant thermal heat flux thermal conditions. 20 nm average diameters of nano particles and 0.1% volume fraction is employed. The numerical analysis includes the numerical simulation of straight tube model by a package ANSYS FLUENT 18 for constant heat flux value of 1×10^4 W/m^2 and the Reynolds number had a range of 6×10^3 to 4×10^4. The consequences displayed that heat transfer coefficient of hybrid fluid was better than that of Al_2O_3-water and pure water by 12% and 23.4% respectively at all Reynolds numbers. The friction factor of hybrid fluid is superior to that of nanofluid and pure water by 4.6% and 11.7% respectively. It found improvement in thermal performance of hybrid fluid compared to that of nanofluids and the pure water. The numerical consequences of Nusselt number values and friction factor magnitudes are validated with the literature consequences obtained and display significant agreement, with a deviation of 7.8 % and 6.4% respectively.

Keywords: nanofluid, pure water, concentration fractio, hybridfluid
Classification numbers: 3.02, 4.15

1. Introduction

A heat exchange between different mediums, such as heat exchangers and fan coils is not a new idea. However, the efficiency of transferring hot water by using pipe system could be affected dramatically by heat loss through the pipe walls to the environment. Based on application, reducing or increasing heat transfer from water pipe system to the environment could positively or negatively improve the efficiency of the water pipe system. Recently, reducing or increasing the heat loss from hot water pipe system can be achieved by using the nanofluid technology. CFM model of straight pipe used with fluid mix of solid nanoparticles and its effect on heat transfer are studied by [1]. The latter study shows that using AlN together with heat flux could improve the heat transfer in straight pipes. The effect of different shaped nanoparticles on temperature loss has been investigated experimentally by [2]. This study concludes that the shape of nanoparticles could play a major role in the heat transfer efficiency from water to the environment. The same outcome is concluded by [3].Turbulent flow and heat transfer characteristics of a twisted heat exchanger with 3-lobed cross section along for Y-tape supplement were studied numerically [4]. Pure water and water-Al_2O_3 nanofluid using two-phase mixture model were used with nanofluid volume fractions of 0.01, 0.02 and 0.03 with Reynolds number in range of 5000–20000. Results displayed that employing the Y-tape twisted tube improves the heat transfer compared to that of the twisted tube. Mohamad *et al* [5] investigated the flow characteristics and heat transfer uses of a helical coil with four different lobed cross sections numerically with laminar flow for Reynolds number range of 1300 to 2500 for constant wall temperature of 100 °C. It can be detected that employing Al_2O_3-water nanofluid leads to increase in the Nusselt number by 28 percent compared to using water only. Mousavi *et al* [6] studied the effect of the magnetic field on heat and

[1] Author to whom any correspondence should be addressed.

 © 2020 Vietnam Academy of Science & Technology

fluid flow of ferrofluid in the helical tube numerically. Results presented that the magnetic field improved Nusselt number by 40%.The hybrid sphere/CNT nanoparticles were synthesised by Han *et al* [7] with a spray pyrolysis method for improving thermal transference in heat transfer fluids. Hybrid nanoparticles are predictable to decrease meaningfully the resistance thermal contact between the CNTs provided that a thermal pathway goes through the center spheres. The hybrid sphere/CNT particles are displayed to increase the oil thermal conductivity about 21% with volume fractions of only 0.2% at room temperature, a greatly higher enhancement in thermal conductivity as compared to simple spheres at the same particle loadings. The convective heat transfer coefficient and friction factor for fully developed turbulent flow of MWCNT–Fe_3O_4/water hybrid nanofluids flowing through a uniformly constant heat flux circular tube are displayed by Syam *et al* [8]. The MWCNT-Fe_3O_4 nanocomposite was equipped via in-situ method that consists of the spreading of carboxylate carbon nanotubes with distilled water and mixing of ferrous chloride and ferric chloride. The heat transfers and friction factor experiments were conducted for particle loadings of 0.1% and 0.3%. The results show a maximum of 31.10% enhancement in Nusselt number with a penalty of 1.18-time rise of pumping power for the particle loading of 0.3% at a Reynolds number of 22000 as compared to base fluid data. Ding *et al* [9] used CNT/water nanofluid and found that enhancement of heat transfer was 350% at 0.5 wt% with Reynolds number of 800. Wang *et al* [10] investigated CNT/water nanofluid and detected heat transfer enhancement of 70% and 190% at 0.05 wt% and 0.24 wt% respectively with Reynolds number of 120. Amrollahi *et al* [11] determined that the increase of heat transfer coefficient for CNT/water nanofluids was 33% and 40% with 0.25 wt% in laminar and turbulent nanofluid flow situations respectively compared with that for pure water in 20 °C temperature, Asirvatham *et al* [12] presented that the water-silver nanofluid oddly increased the heat transfer coefficient by 28.7% and 69.3% for 0.3 wt% and 0.9 wt%, respectively. The idea of employing hybrid nanofluids is to additionally improve heat transfer and pressure drop characteristics by trade-off between advantages and disadvantages of individual interruption, qualify for respectable aspect ratio, improve thermal network and synergistic effect of nanomaterials [13]. Nanofluids were produced by using different weight concentrations of GNP-Ag nanocomposite with distilled water. Experimental measurement presented that thermal conductivity was increased by 22.22% and viscosity increased by 1.3 times at 0.1% particle weight concentration at 40 °C. The Nusselt number was increased in comparison to base fluid [14]. However, full understanding of the mechanism of nanoparticles in improving the heat transfer efficiency is still lacking [15, 16]. Aluminum oxide with high Rayleigh number could decrease the heat transfer when water is used as nanofluid [17]. It has been experimentally concluded that thermal conductivity value could be improved when aluminum oxide or copper oxide is used with 0.2% particle volume as nanoparticles [18]. The objective of this study is to examine heat transfer and hydraulic characteristics development in a straight hexagonal tube by employing the nanofluids of Al_2O_3 and hybrids of (Al_2O_3 and CuO) dispersed in pure water. The CFD examination is achieved via FLUENT 18 program by the finite volume method. The Reynolds numbers, heat flux, and the volume concentration are 6×10^3 to 4×10^4, 10000 Wm^{-2}, and 0.1% respectively.

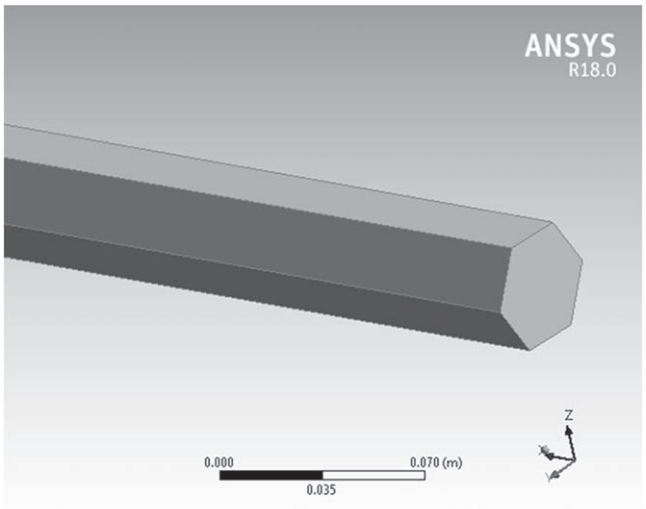

Figure 1. Geometry of model.

2. Numerical model

The numerical analysis was done by CFD (ANSYS FLUENT 18) for the considered geometry. The main governing equations are solved for each cell to evaluate the thermal features and pressure drop of flow. The numerical solution involves a three cylindrical-dimensional geometric model creation, and model mesh is generated through ANSYS 18 program. A straight hexagonal tube is 1000 mm long and has 37 mm internal hydraulic diameter which is shown in figure 1. In the present work, to characterise flow in the numerical simulation, a cylindrical coordinate system (r, θ, z) was used. The assumptions for the present study involve constant heat flux of 10 000 W m^{-2}, turbulent flow, steady state case conditions. Also working fluids is Newtonian with incompressible fluids, neglect tube wall thickness, constant of thermo-physical properties of the nano and hybrids fluids, no influence of gravity, heat conduction mode in axial main path, and no heat source. The inlet boundary conditions of the pure water or nanofluid and hybrid fluids are considered as velocity inlets, while the main outlet boundary conditions are considered as the pressure outlets.

To ensure grid-independent solutions, a number of non-uniform model grids were exposed for testing procedure. The grid node concentrations of 29275, 32768, and 37961 have been established and the consequences of these test cases were compared with the experimental results. The influence of the present number of mesh nodes on Nusselt number of water for hexagonal tube is shown in figure 2. It can be shown that the nearest numerical solution for the experiment is that of the 37961 node as shown in figure 3. There are essentially

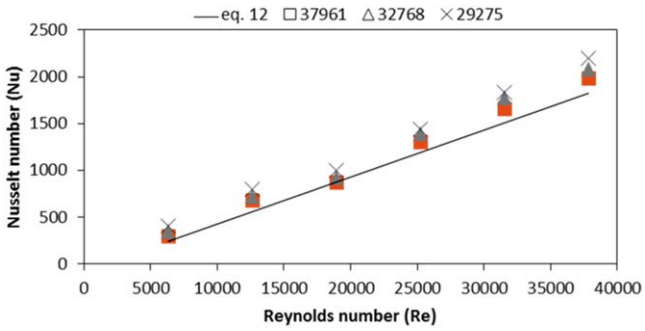

Figure 2. Grid-independent test.

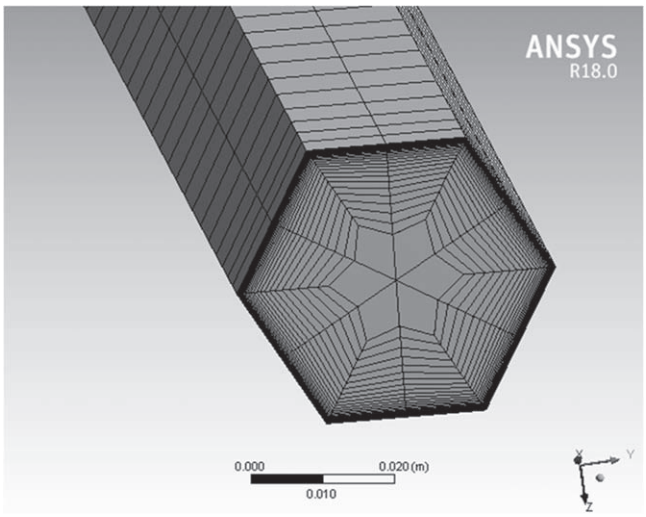

Figure 3. Mesh of model.

two kinds of methodologies in meshing volumes; unstructured and structured meshes. A structured grid is employed in the current model. The main residuals with all governed equations are lower than 10^{-6}.

According to [19, 20], the equation of continuity, momentum and energy is as follows:

$$\frac{1}{r}\frac{\partial(\rho r v_r)}{\partial r} + \frac{1}{r}\frac{\partial(\rho v_\theta)}{\partial \theta} + \frac{\partial(\rho v_z)}{\partial z} = 0. \tag{1}$$

For r, θ, z, it is as follows:

$$v_r\frac{\partial v_r}{\partial_r} + \frac{v_\theta}{r}\frac{\partial v_r}{\partial \theta} + v_z\frac{\partial v_r}{\partial r} - \frac{v_\theta^2}{r} = -\frac{1}{\rho}\frac{\partial p}{\partial r} + \frac{\mu}{\rho} \times\left(\frac{1}{r}\frac{\partial}{\partial r}\left(r\frac{\partial v_r}{\partial r}\right) + \frac{1}{r^2}\frac{\partial^2 v_r}{\partial \theta^2} + \frac{\partial^2 v_r}{\partial z^2}\frac{v_r}{r^2} - \frac{2}{r^2}\frac{\partial v_\theta}{\partial \theta}\right), \tag{2}$$

$$v_r\frac{\partial v_\theta}{\partial_r} + \frac{v_\theta}{r}\frac{\partial v_\theta}{\partial \theta} + v_z\frac{\partial v_\theta}{\partial r} - \frac{v_r v_\theta}{r} = -\frac{1}{\rho}\frac{\partial p}{\partial \theta} + \frac{\mu}{\rho} \times\left(\frac{1}{r}\frac{\partial}{\partial r}\left(r\frac{\partial v_\theta}{\partial r}\right) + \frac{1}{r^2}\frac{\partial^2 v_\theta}{\partial \theta^2} + \frac{\partial^2 v_\theta}{\partial z^2} - \frac{v_\theta}{r^2} - \frac{2}{r^2}\frac{\partial v_r}{\partial \theta}\right), \tag{3}$$

$$v_r\frac{\partial v_z}{\partial_r} + \frac{v_\theta}{r}\frac{\partial v_z}{\partial \theta} + v_z\frac{\partial v_z}{\partial r} = -\frac{1}{\rho}\frac{\partial p}{\partial \theta} + \frac{\mu}{\rho}\left(\frac{1}{r}\frac{\partial}{\partial r}\left(r\frac{\partial v_z}{\partial r}\right) + \frac{1}{r^2}\frac{\partial^2 v_z}{\partial \theta^2} + \frac{\partial^2 v_z}{\partial z^2}\right), \tag{4}$$

$$\rho c_p\left(v_r\frac{\partial T}{\partial r} + \frac{v_\theta}{r}\frac{\partial T}{\partial \theta} + v_z\frac{\partial T}{\partial z}\right) = k\left(\frac{\partial^2 T}{\partial r^2} + \frac{1}{r}\frac{\partial T}{\partial r} + \frac{1}{r^2}\frac{\partial^2 T}{\partial \theta^2} + \frac{\partial^2 T}{\partial z^2}\right). \tag{5}$$

Turbulence model Reynolds-Averaged Navier-Stokes (RANS) governing equations via tensor symbolization were specified via the concluded bar at the bulk velocities are indicated.

$$\frac{\partial \rho}{\partial t} + \frac{\partial \rho U_i}{\partial x_i} = 0, \tag{6}$$

$$\frac{\partial_i}{\partial t}(\rho u_i) + \frac{\partial u}{\partial x_j}(\rho u_i u_j) = -\frac{\partial P}{\partial x_i} + \frac{\partial}{\partial x_i} \times\left[\mu\left(\frac{\partial u_i}{\partial x_j} + \frac{\partial u_j}{\partial x_i} - \frac{2}{3}\delta_{ij}\frac{\partial u_i}{\partial x_i}\right)\right] + \frac{\partial}{\partial x_j}(\overline{\rho u'_i u'_j}). \tag{7}$$

The two main turbulence model equations are solved transported equations to characterise a turbulent possession and develop an eddy viscosity. This permits the models with description of the effects of convection mode and diffusion mode of the main turbulent vitality. The transported main variable was the turbulence model kinetic energy K with a specific dissipation ε for K-ε model. The mean transport variable governs energy within turbulence with other variables and governs the main turbulence scale which is defined as [21]:

$$\frac{\partial(\rho k)}{\partial t} + \frac{\partial}{\partial x_j}(\rho U_{jk}) = \frac{\partial}{\partial x_j}\left[\left(\mu + \frac{\mu_t}{\sigma_k}\right)\frac{\partial k}{\partial x_j}\right] + P_k - \rho\varepsilon + P_{kb}, \tag{8}$$

$$\frac{\partial(\rho \varepsilon)}{\partial t} + \frac{\partial}{\partial x_j}(\rho U_{j\varepsilon}) = \frac{\partial}{\partial x_j}\left[\left(\mu + \frac{\mu_t}{\sigma_\varepsilon}\right)\frac{\partial \varepsilon}{\partial x_j}\right] + \frac{\varepsilon}{k}(c_{\varepsilon_1}P_k - c_{\varepsilon_2}\rho\varepsilon + c_{\varepsilon_3}P_{\varepsilon b}). \tag{9}$$

Where $C_{\varepsilon_1} = 1.44$, $C_{\varepsilon_2} = 1.92$ and $\sigma_k = 1$. P_{kb} and $P_{\varepsilon b}$ symbolise the effect of the main buoyancy forces. P_k represented the production of turbulence as a result of forces of viscosity, which is displayed by:

$$\frac{\partial(\rho k)}{\partial t} + \frac{\partial}{\partial x_j}(\rho U_{jk}) = \frac{\partial}{\partial x_j}\left[\left(\mu + \frac{\mu_t}{\sigma_k}\right)\frac{\partial k}{\partial x_j}\right] + P_k - \rho\varepsilon + P_{kb}, \tag{10}$$

The K-ε model represented the viscosity of turbulence which is connected to the turbulence kinetic energy and the dissipation as [21]:

$$\mu_t = C_\mu \rho \frac{k^2}{\varepsilon}. \tag{11}$$

Where $C_\mu = 0.09$.

The forced convection mode heat transfer coefficient for turbulent flow might be expected according to [22] via equation (3) for the main base fluid and Reynolds number

Table 1. The hybrid and nanofluid properties.

Fluid	Volume fraction (%)	Density (Kg m^{-3})	Specific heat (J/kg K)	Thermal conductivity (W/m.K)	Dynamic viscosity (N.s m^{-2})
AL2O3-water	0.1	1040	4322	1.03	0.002
(AL2O3 + CuO)-water	0.1	1140	4700	1.08	0.003
Water	—	995.8	4178.4	0.615	0.0008

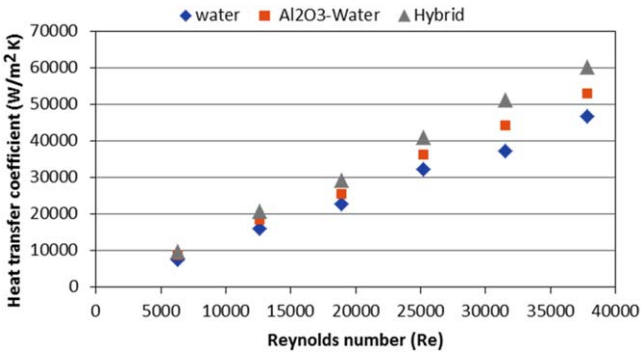

Figure 4. Heat transfer coefficient of pure water, Al_2O_3 plus water and (Al_2O_3+CuO) plus water.

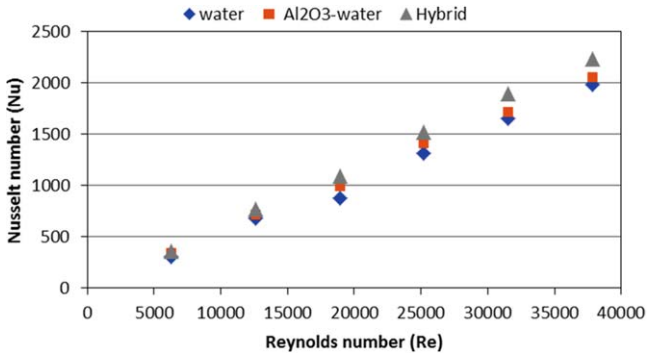

Figure 5. Nusselt number of pure water, Al_2O_3 plus water and (Al_2O_3+CuO) plus water.

range of $5 \times 10^3 < \mathrm{Re} < 10^5$.

$$Nu = \frac{h_f}{k_f} D = 0.023\,\mathrm{Re}^{0.8}\,\mathrm{Pr}^{0.4}. \tag{12}$$

The friction factor of the main base fluid inside the straight tube is defined as [23]:

$$f_f = 0.3164/\,\mathrm{Re}^{0.25}. \tag{13}$$

The friction factor for the nanofluid inside the straight tube from experimental tests is defined as [24]:

$$\frac{f_{nf}}{f_f} = 1.075\left(\frac{\rho_{nf}}{\rho_f}\right)^{-0.514}\left(\frac{\mu_{nf}}{\mu_f}\right)^{-0.1248}. \tag{14}$$

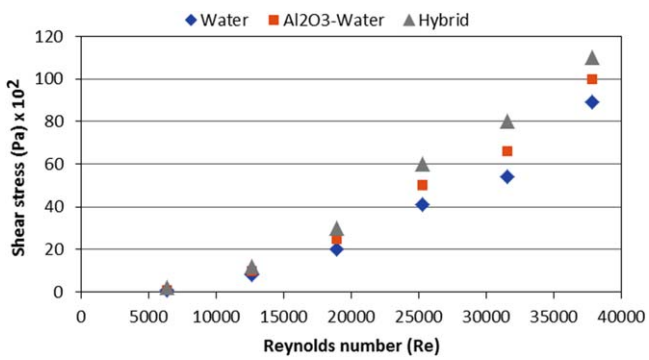

Figure 6. Shear stress of pure water, Al_2O_3 plus water and (Al_2O_3+CuO) plus water.

3. Properties of nanofluids

The properties of solid CuO and AL2O3 particles which are used in the present work are constant value of 293 K to 323 K. The present simulations involve features of nanofluids and hybrid fluids with dependent temperature. Table 1 displays the nanofluid and hybrid fluid features of CuO-water and (Al_2O_3 + CuO)-water at the hexagonal tube inlet section. The nanofluid obtainable equations were considered by employing the [25] relationships that are defined as:

$$\rho_{nf} = (1 - \Phi)\rho_f + \Phi\rho_p. \tag{15}$$

Where ρ_{nf} represents the nanofluid density, Φ represents the volume concentration of particles, ρ_f represents the main base fluid density and ρ_p represents the nanoparticle density. The

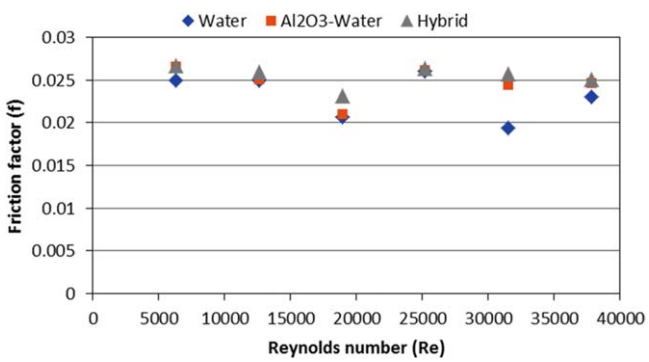

Figure 7. Friction factor for pure water, Al_2O_3 plus water and (Al_2O_3+CuO) plus water.

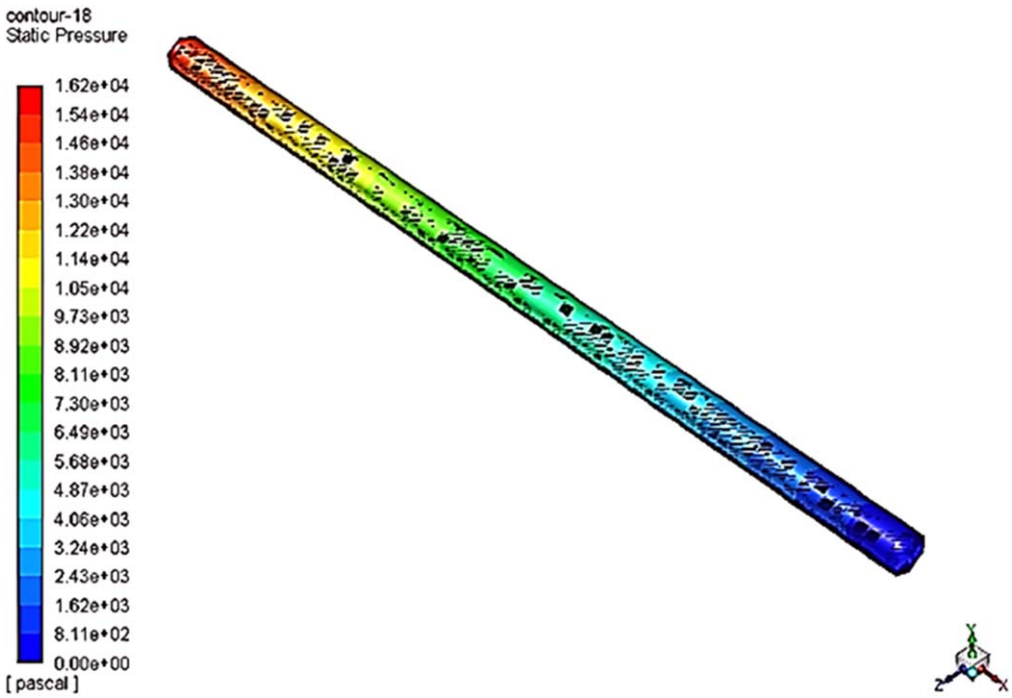

Figure 8. Pressure drop distribution contour for (Al_2O_3 + CuO)-water.

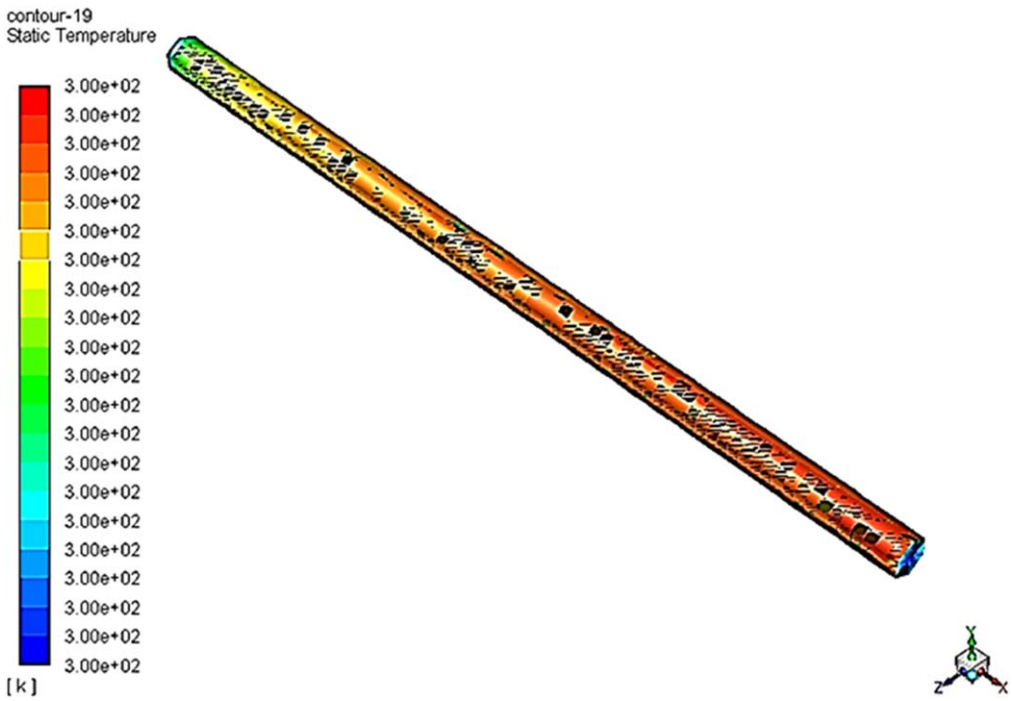

Figure 9. Static temperature distribution contour for (Al_2O_3 + CuO)-water.

specific heat is considered from [26] as:

$$(\rho C_p)_{nf} = (1 - \Phi)(\rho C_p)_f + \Phi(\rho C_p)_p. \tag{16}$$

Where Cp_{nf} represents the nanofluid heat capacity, Cp_f represents the base fluid heat capacity and Cp_p represents the nanoparticle heat capacity. A substitute formulation for computing the thermal conductivity is presented by [27] as:

$$K_{nf} = K_f \frac{K + 2K_f - 2\Phi(K_f - K)}{K + 2K_f + \Phi(K_f + K)}. \tag{17a}$$

Where K_{nf} represents the nanofluid thermal conductivity, K represents the nanoparticle thermal conductivity and K_f

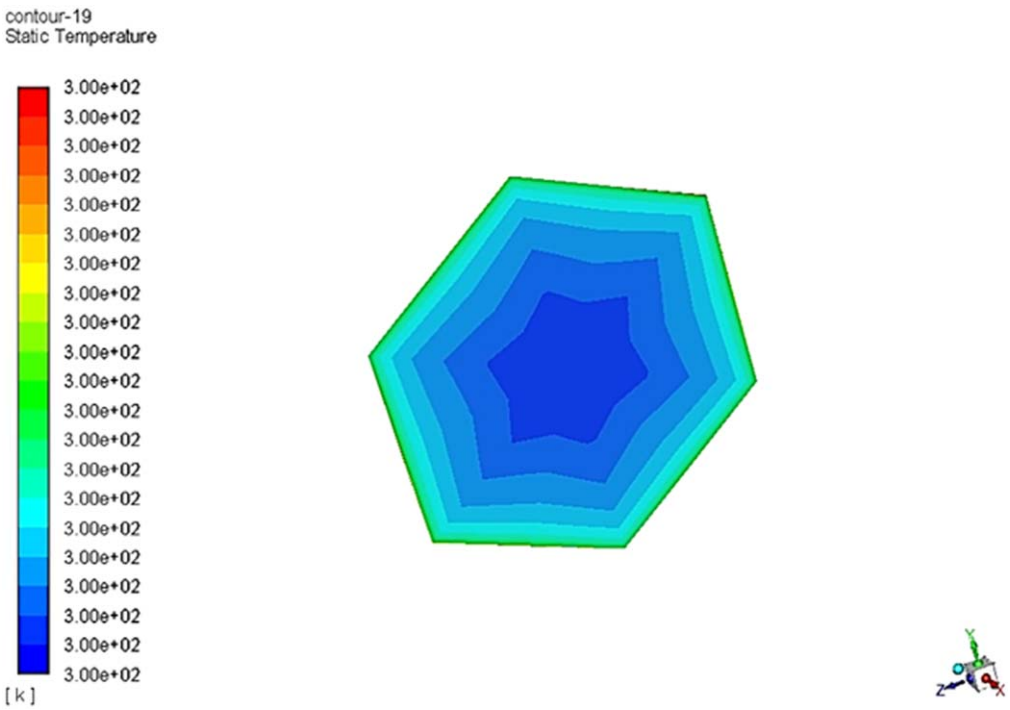

Figure 10. Static temperature contour distribution at outlet for (Al_2O_3 + CuO)-water.

represents the main base fluid thermal conductivity. Previous research [28] recommended the identified Einstein's equation to compute viscosity of nanofluids as:

$$\mu_{nf} = (1 + 2.5\Phi)\mu_w. \tag{17b}$$

Where μ_{nf} represents the viscosity of nanofluid and μ_w represents the viscosity of water. The hybrid and nanofluid properties displayed in the above equations were estimated from nanoparticles and water at room temperature as shown in table 1. For uncertainty analyses see appendix B.

In this study, nanoparticles of about 30 nm diameter are used. Nanofluids are generally considered to be stable if the concentration of the supernatant particles remains constant with time. Sedimentation method is used [29]. An external force field is applied to start the sedimentation of nanoparticles in the nanofluids. The weight of sediment or the volume of sediment indicates the stability of nanofluids [29].

4. Results

The validation of the data is shown in appendix C. Figure 4 displays a comparison of CFD analysis consequences of the heat transfer coefficient for the pure water, Al_2O_3 plus water and hybrid (Al_2O_3+CuO) plus water for the turbulent model flow conditions. It could be shown that heat transfer coefficients for hybrids fluid are superior to that of Al_2O_3 plus water and pure water by 12 and 23.4% respectively, due to increasing hybrid fluids thermal conductivity.

Figure 5 displays the comparison of CFD analysis consequences of Nusselt number of pure water, Al_2O_3-water and

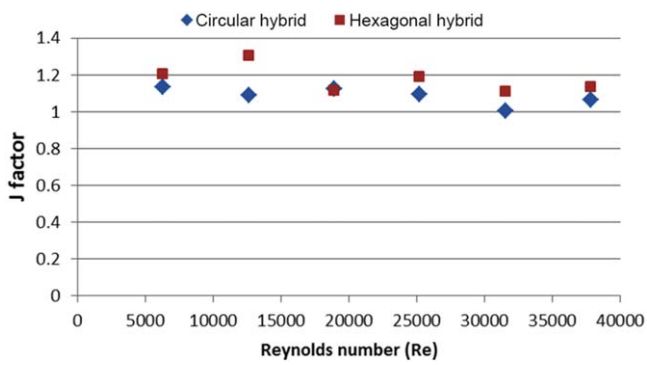

Figure 11. *J* factor of (Al_2O_3 + CuO)-water for hexagonal and circular tubes.

hybrid fluid (Al_2O_3 + CuO)-water under turbulent flow conditions. It could be shown that Nusselt number of hybrid fluid was higher than that of Al_2O_3-water nanofluid and pure water due to increasing hybrid fluid thermal conductivity.

Figure 6 displays the shear stress and the Reynolds number of pure water, Al_2O_3-water and (Al_2O_3 + CuO)-water for 0.1% volume concentration fraction. It could be shown that shear stress of hybrid fluid was higher than that of Al_2O_3-water nanofluid and pure water by 24.9% and 37% respectively due to increasing hybrid fluid viscosity.

Figure 7 displays the friction factor and the Reynolds number of pure water, Al_2O_3-water and (Al_2O_3 + CuO)-water for 0.1% volume concentration fraction. The influence of the hybrid fluid is insignificant. The friction factor decreases with the rise of the Reynolds number. The friction factor of hybrid fluid is superior to that of nanofluid and pure water by 4.6%

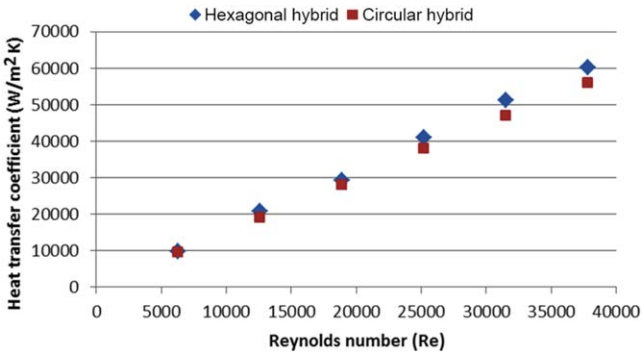

Figure 12. Heat transfer coefficient of (Al_2O_3 + CuO)-water for hexagonal and circular tubes.

and 11.7% respectively due to increasing hybrid fluid viscosity [30].

Figure 8 displays the pressure drop contour distribution for (Al_2O_3 + CuO)-water at 4×10^4. Figures 9 and 10 display the temperature contour distribution for (Al_2O_3 + CuO)-water at 4×10^4. The consequential information displays that the hybrid fluid temperature is increased with length of tube as a result of adding heat. For figures 9 and 10, it should be noted that the change in temperature is less than 1 °K. Therefore, it does not appear in legend.

Hexagonal duct is modified for enhancing heat transfer and results are compared with the circular, square and regularly hexagonal tube of equal cross section. In this study, more analyses are done for three cases of mass flow rate. Heat transfer, temperature change, heat transfer coefficient and pressure drop are numerically analysed by using ANSYS 14.5. Comparison result indicates that the modified hexagon transfers the maximum amount of heat, which is subjected to the highest heat transfer coefficient, use of modified hexagon can improve the effectiveness and efficiency of a heat exchanger. Comparison result also signifies that *J* factor of hexagonal tube and heat transfer coefficient shown in figures 11 and 12 have the highest magnitudes compared with circular tube for the same values of Reynolds number; therefore, use of hexagon can improve the thermal performance.

5. Conclusions

A numerical investigation into the effect of Al_2O_3 nanopowder and hybrids of (Al_2O_3 and CuO) powders dispersed in pure water in straight tube with hexagonal cross section form on the pressure drop and thermal performance is presented in this work. The range of Reynolds numbers considered is 6×10^3 to 4×10^4. This study considered forced convection mode heat transfer with turbulent flow model with the constant heat flux main boundary conditions of 20 nm average diameter of nanoparticles and 0.1% volume fraction. The friction factor of hybrid fluid is superior to that of nanofluid and pure water by 4.6% and 11.7% respectively. It found improvement in thermal performance of hybrid fluid compared to that of nanofluids and the pure water.

Appendix A. Nomenclature and symbols

C_p	specific heat, J/kg K	Φ	volume concentration, %
d	nanoparticle diameter, m	ρ	density, kg/m^3
D	tube diameter, m	α	thermal diffusivity, m^2/s
f	friction factor	μ	viscosity, kg/ms
U	overall heat transfer coefficient, W/m^2 K	ΔT	1 °C
K	thermal conductivity, W/mK	wi	water inlet
m	mass flow rate, L/s	wo	water outlet
Nu	Nusselt number	ni	nanofluid inlet
Re	Reynolds number	no	nanofluid outlet
Pe	Peclet number	in	inlet
Pr	Prandtl number	out	outlet
T	temperature, °C	n	nanofluid
V	mean velocity, m/s	f	base fluid
υ	kinematic viscosity, m^2/s	ρ	nanoparticles
Q	heat transfer, W		

Appendix B. Uncertainty analysis

All the quantities that were measured to estimate the Nusselt number and the friction factor are subjected to uncertainties due to error in measurement. Uncertainty analysis is carried out using Coleman and Steele method [31] which considers the measurement errors. For this purpose, quantities like the tube diameter (d), length of the test section (L), mass flow rate (m), pressure drop (Dp), voltage (V), current (I), wall temperature (T_w), fluid average temperature (T_f), fluid thermal conductivity (k), viscosity (l) are measured and the probable errors in each of them are calculated to estimate the uncertainties associated with experimental data of friction factor and Nusselt number. Experimental uncertainty was calculated according to ANSI/ASME standards [32]. The uncertainties associated with experimental data are calculated on the basis of 95% confidence level. The calculations indicated that the uncertainties involved in the measurements are around ±3%, ±5% and ±5% respectively for Reynolds number, Nusselt number and friction factor.

Appendix C. Validation of data

Figure C1 illustrates the comparisons of the numerical results for present study and established experimental results [8] for the Nusselt number using hybrid nanofluid for the same range of Reynolds numbers. The Nusselt number increases as the Reynolds number increases with the deviation of 16%.

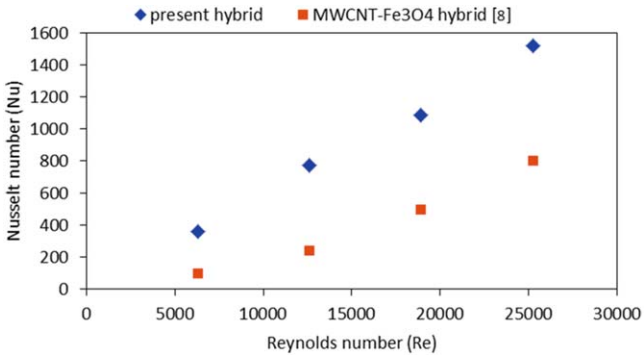

Figure C1. Validation of results for Nusselt number.

References

[1] Hussein A M, Noor M, Kadirgama K, Ramasamy D and Rahman M 2017 *International Journal of Automotive & Mechanical Engineering* **14** 4183–95

[2] Babar H, Sajid M and Ali H M 2019 *Therm. Sci.* **23** 1713–54

[3] Zhou S-Q and Ni R 2008 *Applied Physics Letters* **92** 093123

[4] Omidi M, Darzi A A R and Farhadi M 2019 *Journal of Thermal Analysis and Calorimetry* **137** 1451–62

[5] Omidi M, Farhadi M and Darzi A A R 2018 *Energy conversion and management* **176** 236–45

[6] Mousavi S, Jamshidi N and Rabienataj-Darzi A 2019 *Journal of Thermal Analysis and Calorimetry* **137** 1591–601

[7] Han Z, Yang B, Kim S and Zachariah M 2007 *Nanotechnology* **18** 105701

[8] Sundar L S, Singh M K and Sousa A C 2014 *International Communications in Heat and Mass Transfer* **52** 73–83

[9] Ding Y, Alias H, Wen D and Williams R A 2006 *International Journal of Heat and Mass Transfer* **49** 240–50

[10] Wang J, Zhu J, Zhang X and Chen Y 2013 *Experimental Thermal and Fluid Science* **44** 716–21

[11] Amrollahi A, Rashidi A, Lotfi R, Meibodi M E and Kashefi K 2010 *International Communications in Heat and Mass Transfer* **37** 717–23

[12] Asirvatham L G, Raja B, Lal D M and Wongwises S 2011 *Particuology* **9** 626–31

[13] Sarkar J, Ghosh P and Adil A 2015 *Renewable and Sustainable Energy Reviews* **43** 164–77

[14] Yarmand H, Gharehkhani S, Ahmadi G, Shirazi S F S, Baradaran S, Montazer E *et al* 2015 *Energy Conversion and Management* **100** 419–28

[15] Sundar L S, Sharma K, Singh M K and Sousa A 2017 *Renewable and Sustainable Energy Reviews* **68** 185–98

[16] Aich N, Plazas-Tuttle J, Lead J R and Saleh N B 2014 *Environmental Chemistry* **11** 609–23

[17] Ghasemi B and Aminossadati S 2009 *Numerical Heat Transfer, Part A: Applications* **55** 807–23

[18] Senthilraja S, Vijayakumar K and Gangadevi R 2015 A comparative study on thermal conductivity ofAl_2O_3/water, CuO/water and Al_2O_3–CuO/water nanofluids *Digest Journal of Nanomaterials and Biostructures* **10** 1449–58

[19] Bird R B, Armstrong R C and Hassager O 1987 *Fluid Mechanics. Dynamics of Polymeric Liquids* **vol 1**

[20] White F 1991 *Viscous Fluid Flow* 2nd ed. (New York, USA: McGrawHill)

[21] Bhaskaran R and Collins L 2002 Introduction to CFD Basics *Cornell University-Sibley School of Mechanical and Aerospace EngineeringIntroduction to CFD Basics* 101–17

[22] Dittus F W 1930 Heat transfer in automobile radiators of the tubler type *Univ. Calif. Pubs. Eng.* **2** 443

[23] Blasius H 1913 *In Mitteilungen über Forschungsarbeiten auf dem Gebiete des Ingenieurwesens* (Berlin: Springer) 1–41 (https://link.springer.com/chapter/10.1007/978-3-662-02239-9_1)

[24] Duangthongsuk W and Wongwises S 2009 *International Journal of Heat and Mass Transfer* **52** 2059–67

[25] Pak B C and Cho Y I 1998 *Experimental Heat Transfer an International Journal* **11** 151–70

[26] Xuan Y and Roetzel W 2000 *International Journal of Heat and Mass Transfer* **43** 3701–7

[27] Yu W and Choi S 2003 *Journal of Nanoparticle Research* **5** 167–71

[28] Drew D A and Passman S L 2006 *Theory of Multicomponent Fluids* (Springer Science & Business Media) **135**

[29] Wei X and Wang L 2010 *Particuology* **8** 262–71

[30] Azmi W, Sharma K, Sarma P, Mamat R, Anuar S and Sundar L S 2014 *Applied Thermal Engineering* **73** 296–306

[31] Coleman, H W and Steele W 1989 *Experimental and Uncertainty Analysis for Engineers* (New York: Wiley)

[32] Abernethy R B, Benedict R P and Dowdel R B 1985 ASME measurement uncertainty *Journal of Fluids Engineering* **107** 161–4